

# On the evolution of low-mass central galaxies in the vicinity of massive structures

Daniela Palma<sup>1</sup>, Ivan Lacerna<sup>1,2</sup>, M. Celeste Artale<sup>3</sup>, Antonio D. Montero-Dorta<sup>4</sup>, Andrés N. Ruiz<sup>5,6</sup>, Sofía A. Cora<sup>7,8</sup>, Facundo Rodriguez<sup>5,6</sup>, Diego Pallero<sup>9</sup>, Ana O’Mill<sup>5,6</sup>, and Nelvy Choque-Challapa<sup>1,4</sup>

<sup>1</sup> Instituto de Astronomía y Ciencias Planetarias de Atacama, Universidad de Atacama, Copayapu 485, Copiapó, Chile.  
e-mail: daniela.palma@postgrados.uda.cl

<sup>2</sup> Millennium Institute of Astrophysics, Nuncio Monsenor Sotero Sanz 100, Of. 104, Providencia, Santiago, Chile.

<sup>3</sup> Universidad Andres Bello, Facultad de Ciencias Exactas, Departamento de Ciencias Físicas, Instituto de Astrofísica, Av. Fernández Concha 700, Santiago, Chile.

<sup>4</sup> Departamento de Física, Universidad Técnica Federico Santa María, Av. Vicuña Mackenna 3939, 8940897, San Joaquín, Santiago, Chile.

<sup>5</sup> CONICET. Instituto de Astronomía Teórica y Experimental (IATE). Laprida 854, Córdoba X5000BGR, Argentina.

<sup>6</sup> Universidad Nacional de Córdoba (UNC). Observatorio Astronómico de Córdoba (OAC). Laprida 854, Córdoba X5000BGR, Argentina.

<sup>7</sup> Instituto de Astrofísica de La Plata (CCT La Plata, CONICET, UNLP), Paseo del Bosque s/n, La Plata, Argentina.

<sup>8</sup> Facultad de Ciencias Astronómicas y Geofísicas, Universidad Nacional de La Plata, Paseo del Bosque s/n, La Plata, Argentina.

<sup>9</sup> Departamento de Física, Universidad Técnica Federico Santa María, Avenida España 1600, Valparaíso, Chile.

Received –; accepted –

## ABSTRACT

We investigate the population of low-mass central galaxies with  $M_{\star} = 10^{9.5} - 10^{10} h^{-1} M_{\odot}$ , inhabiting regions near massive groups and clusters of galaxies using the IllustrisTNG300 and MDPL2-SAG simulations. We set out to study their evolutionary histories, aiming to find hints about the large-scale conformity signal they produce. We also use a control sample with the same stellar mass range to distinguish the evolution of central galaxies located far away from massive structures. For both samples, we find a sub-population of galaxies that were accreted by another halo in the past but are now considered central galaxies; we refer to these objects as former satellites. The number of former satellites is higher for quenched central galaxies in the vicinity of massive systems, with fractions of 45% and 17% in IllustrisTNG300 and MDPL2-SAG simulations, respectively. Our results in TNG300 show that former satellites were typically hosted by massive dark matter halos ( $M_{200} \geq 10^{13} h^{-1} M_{\odot}$ ) at  $z \sim 0.3$ , followed by a drop in halo mass at lower redshifts. In addition, we find a strong drop in the total gas mass at  $z \leq 1$  for quenched central galaxies in the vicinity of galaxy groups and clusters produced by these former satellites as well. After removing former satellites, the evolutionary trends for quenched central galaxies are fairly similar to those of the quenched control galaxies, showing small differences at low redshift. For MDPL2-SAG instead, former satellites were hosted by less massive halos, with a mean halo mass around  $10^{11} h^{-1} M_{\odot}$ , and the evolutionary trends remain equal before and after removing former satellite galaxies. We also measure the two-halo conformity, i.e., the correlation in the specific star formation rate between low-mass central galaxies and their neighbors at Mpc scales, and how former satellites contribute to the signal at three different redshifts:  $z = 0, 0.3$ , and 1. The time evolution of the conformity signal is apparently contradictory in both simulations, it decreases from  $z = 0$  to  $z = 1$  in MDPL2-SAG, while it increases in TNG300. However, after removing former satellites in the latter, the signal is strongly reduced but practically does not change at  $z \leq 0.3$ , and it disappears at  $z = 1$ . We compare our findings with recent literature and discuss the conformity measurements, as different approaches can lead to varying results.

**Key words.** Galaxies: evolution – Galaxies: halos – Galaxies: groups: general – Galaxies: clusters: Galaxies: star formation – general – Methods: numerical

## 1. Introduction

The processes that cause the quenching of star formation in galaxies are still not fully understood. On one side, there are internal effects related to the feedback produced by supernovae (SNe) and active galactic nuclei (AGN) that contribute to the star formation quenching. On the other side, we know that inside galaxy clusters several environmental effects can occur such as ram-pressure stripping (RPS, Gunn & Gott 1972; Forman & Jones 1982; Giovanelli & Haynes 1985; Aragon-Salamanca et al. 1993), which can strip the hot and cold gas, being stronger at distances closer to the halo center. Galaxy encounters or harassment (Moore et al. 1996; Moore et al. 1998) are also likely to occur to shut down the star formation activity. Starvation, when

the accretion of gas is ceased due to lack of gas supply (Larson et al. 1980; McCarthy et al. 2008; Peng et al. 2015), and tidal forces produced by the potential well of the halo (Moore et al. 1999; Newberg et al. 2002; McCarthy et al. 2008; Villalobos et al. 2014) can contribute as well. Man & Belli (2018) provide a concise overview and a comprehensive classification of the quenching mechanisms in massive galaxies, highlighting the diverse physical processes that disturb the balance between gas accretion and ejection, consequently impacting the reservoir of cold gas available for star formation. Some environmental effects can extend to the vicinity of clusters up to scales of several Mpc; an example of this is pre-processing (Fujita 2004; Wetzel et al. 2013; Haines et al. 2015; Pallero et al. 2019; Hough et al.

2023; Piraino-Cerda et al. 2024) that occurs before galaxies enter galaxy clusters, showing a reduction in their star formation activity. The main mechanism responsible for pre-processing is RPS that acts within clusters or groups (Tecce et al. 2010), but also outside galaxy clusters (e.g., Bahé et al. 2013; Ayromlou et al. 2021). Galaxies may undergo pre-processing once or several times during their lifetime, leading to the removal of hot (Abadi et al. 1999) and cold (Balogh et al. 2000) gas reservoirs. The efficiency of this removal can be associated with the mass of the halo that hosts these galaxies (Lopes et al. 2024). Bahé et al. (2013) studied the environmental effects outside galaxy clusters in the GIMIC cosmological hydrodynamic simulations at  $z \sim 0$ . In particular, they considered galaxies with stellar masses between  $\log_{10}(M_{\star}/M_{\odot}) = [9.0, 11.0]$ . For the whole mass range studied, they found a fraction of pre-processed galaxies located at large cluster-centric distances (up to four virial radii). In addition, they showed that RPS is efficient in removing the hot gas halo around all the galaxies studied up to several virial radii (see also Zinger et al. 2018 for quenching of satellites at the outskirts of clusters). In contrast, only for less massive galaxies ( $\log_{10}(M_{\star}/M_{\odot}) < 10^{9.5}$ ), the RPS can also remove the cold gas near the massive clusters. Lopes et al. (2024) found that galaxy groups near clusters in the Sloan Digital Sky Survey (SDSS) can quench star formation activity in galaxies even at cluster-centric distances up to five virial radii. Their findings demonstrate a dependency of the pre-processing effect on group mass, with massive halos leading to a more significant suppression of star formation activity compared to low-mass halos (see also Wang et al. 2007; Hahn et al. 2009). In this scenario, less massive galaxies are more susceptible to suffering these large-scale environmental effects before entering a more massive group or cluster (Bahé et al. 2013, Ayromlou et al. 2021). Salerno et al. (2022) studied different galaxy environments to analyze the star formation quenching using the MDPL2-SAG galaxy catalog (Knebe et al. 2018), obtained from the combination of the semi-analytic model SAG Cora et al. (2018) and the dark matter only cosmological simulation MULTIDARK PLANCK 2, MDPL2 (Klypin et al. 2016). In particular, they considered three galaxy types related to their location: cluster galaxies (CG), galaxies in the filamentary infall region (FRG), and in isotropic infall region (IRG) at three different redshifts:  $z = 0, 0.65$  and  $0.85$ . They found that the red fraction predominates for FRG over IRG at clustercentric distances greater than  $\sim 3$  virial radii, regardless of stellar mass. Furthermore, they observed that across the entire redshift range analyzed, star formation quenching is more pronounced in filamentary regions than in isotropic infall regions. Additionally, they analyzed the evolution of hot gas for these galaxies, finding that hot gas in infall and filamentary regions grows up  $z \sim 0.5$  and then decreases. In contrast, field galaxies show a monotonic increase with a slight decrease at  $z = 0$ . Their results showed the importance of filamentary regions in acting more efficiently in pre-processing galaxies along their evolution (see also Sarron et al. 2019).

Using the same galaxy catalog, Hough et al. (2023) studied four populations of galaxies based on their orbits in and around relaxed clusters: recent and ancient infallers, and backsplash and neighbor galaxies. They found that around  $\sim 65\%$  of quenched galaxies are backsplash, that is, galaxies that at  $z = 0$  are located at distances larger than the virial radius of a cluster, but in the past, they were part of the cluster at some time; these galaxies constitute the dominant population in the outskirts of clusters (up to  $\sim 3$  virial radii). Their findings suggest that around 70% of passive backsplash experienced pre-processing effects. On the contrary,  $\sim 65\%$  of star-forming backsplash galaxies did

not show evidence of pre-processing effects. In a recent paper by Ruiz et al. (2023) the quenching of star formation is studied at different stages of the dynamical evolution of a galaxy. They found that the environmental effects of a cluster can affect galaxies that cross the virial radius of the cluster after a single passage, with low-mass galaxies ( $< 3 \times 10^{10} h^{-1} M_{\odot}$  at  $z = 0$ ) orbiting close through the cluster center being the most affected. In the literature, when galaxies cross the virial radius of a more massive system, e.g., a galaxy cluster, once or several times during their lifetimes, and they are later located outside the virial radius of that dark matter halo, they are commonly referred to as backsplash, fly-by, or former satellite galaxies (e.g., Salerno et al. 2022; Ayromlou et al. 2023 Hough et al. 2023; Ruiz et al. 2023). The first two definitions consider the trajectory of these galaxies (see Ayromlou et al. 2023), being backsplash galaxies those that cross the virial radius and at some time will fall back into the potential well of the cluster; fly-by galaxies on the other hand, are those galaxies that due to their elliptical orbits passed the virial radius only once. We will widely refer to the galaxies in both cases as former satellites. Most of the works cited above on galaxies in the outskirts of clusters do not separate between central and satellite galaxies, where the centrals reside near the center of the potential well of host dark matter halos. Central galaxies are hosted by halos of different masses, including low-mass systems. Wetzel et al. (2012) tested how the fraction of quenched galaxies from the SDSS Data Release 7 (DR7, Blanton et al. 2005; Abazajian et al. 2009) changes at different cluster-centric distances splitting the galaxies into centrals and satellites. Their results showed a significantly higher fraction of central quenched galaxies at two virial radii compared to the field centrals, suggesting a non-negligible fraction of quenched, low-mass central galaxies inhabiting the outskirts of massive systems.

On the other hand, it has been shown that low-mass central galaxies can exhibit strong two-halo conformity, which is the correlation in color or star formation rate (SFR) between central galaxies and their neighbors (e.g., Lacerna et al. 2022, Ayromlou et al. 2023, Wang et al. 2023). Lacerna et al. (2022) measured the conformity signal using the hydrodynamical simulation IllustrisTNG300 (Weinberger et al. 2017; Pillepich et al. 2018) and two catalogs from the semi-analytic model SAG applied to the MDPL2 simulation, that differ in the redshift dependence of the SNe feedback efficiency. They found that low-mass central galaxies in the outskirts of massive systems lead to strong conformity at several Mpc scales at  $z = 0$ . As mentioned above, some environmental effects could be acting beyond the virial radius of galaxy clusters, so we could assume that these effects may be contributing to the signal by quenching the galaxies around them. Therefore, a deeper analysis needs to be performed. A recent study performed by Ayromlou et al. (2023) using the semi-analytical galaxy evolution model, L-GALAXIES, the hydrodynamical simulations IllustrisTNG and EAGLE, and SDSS and DESI observations found that the conformity signal at large scales could be produced by these large-scale environmental effects, such as RPS acting on satellites beyond the halo boundary and on central galaxies in the outskirts of massive halos. They also measured the contribution of ‘former satellite’ galaxies, using the L-GALAXIES semi-analytic model. They found that these galaxies contributed between 0 - 20% to the conformity signal. On the other side, using IllustrisTNG300 Wang et al. (2023) found that former satellites (the term backsplash galaxies is used) can explain the whole signal at  $z = 0$ . However, they considered only centrals as neighbor galaxies, excluding satellites which modifies the classical definition of the two-halo conformity.

These studies highlight the importance of the former satellite definition which can lead to different results. In order to understand the origin and the impact of former satellites on the two-halo conformity signal, we analyze the galaxy population generated by a hydrodynamical simulation (IllustrisTNG300) and by a semi-analytic model of galaxy formation (SAG), to study the evolutionary histories of low-mass central galaxies located in the outskirts of massive clusters or groups.

Then, we analyze the impact of former satellites on the two-halo conformity at three different epochs, emphasizing the importance of a robust definition of these type of galaxies to understand their role. We also report different results when former satellites were accreted by massive and non-massive systems.

The paper is organized as follows. In Section 2, we describe both hydrodynamical and semi-analytic data to be used. The samples are described in Section 3. Our results about the evolution of low-mass central galaxies are presented in Section 4, while the two-halo conformity signal at three epochs is shown in Section 5. Our discussions and main conclusions are presented in Section 6.

## 2. Data

For the purpose of this work, we will use the suite of hydrodynamical cosmological simulations ILLUSTRISTNG and a semi-analytic galaxy catalog MDPL2-SAG, built from the galaxy formation model SAG. The reason for using them is that both datasets revealed a strong two-halo conformity at redshift  $z = 0$  in low-mass central galaxies near massive systems, making them good models for studying this signal at higher redshifts. Recent works have also shown that semi-analytic and hydrodynamical models can address different results related to former satellites on conformity (see Ayromlou et al. 2023, Wang et al. 2023). Thus, we expect to contribute to the discussion of previous results with our definition of former satellites in both simulations (see Sect. 3.4).

The advantage of using a hydrodynamical model is that all the physical processes and environmental effects can act on central and satellite galaxies throughout their evolution. This provides tools to estimate environmental effects that galaxies may suffer, without distinguishing their type. On the other hand, a semi-analytic model (SAM) could help us to trace the evolution of some parameters that are not directly obtained in hydrodynamical models, such as the contribution of cold- and hot gas separately. Furthermore, Lacerna et al. (2022) observed that the MDPL2-SAG model produces results qualitatively similar to those of TNG300 regarding the conformity signal. Therefore, the SAG model will be useful for understanding the environmental processes these galaxies may have undergone in the past to produce the observed conformity signal. This is because environmental effects such as RPS are only applied to satellite galaxies and not to centrals in the SAG model. In addition, SAM offers a larger box size, leading to a significant fraction of galaxies in all mass ranges, providing very good statistics. The following subsection provides a detailed description of the datasets employed in this work. Both datasets are summarized in Table 1.

### 2.1. IllustrisTNG

The IllustrisTNG project (Naiman et al. 2018; Nelson et al. 2018; Marinacci et al. 2018; Pillepich et al. 2018; Springel et al. 2018; Nelson et al. 2019) is a set of cosmological magnetohy-

	TNG300	MDPL2-SAG
Volume	$(205 h^{-1} \text{ Mpc})^3$	$(1 h^{-1} \text{ Gpc})^3$
$N_{\text{gas}}$	$2500^3$	-
$N_{\text{DM}}$	$2500^3$	$3840^3$
$m_{\text{baryon}}$	$7.451 \times 10^6 h^{-1} M_{\odot}$	-
$m_{\text{DM}}$	$3.996 \times 10^7 h^{-1} M_{\odot}$	$1.5 \times 10^9 h^{-1} M_{\odot}$

**Table 1.** Properties of the IllustrisTNG300 simulation and MDPL2-SAG model.

drodynamic simulations, TNG50, TNG100, and TNG300, presented in three different volumes (and resolutions), corresponding to 51.7, 110.7, and 302.6 Mpc of box length, respectively. These simulations solve the equations of gravity and magnetohydrodynamics using the moving-mesh code Arepo (Springel 2010). The model includes the contribution of a wide range of physical processes such as radiative cooling, star formation, supernova and AGN feedback, and chemical enrichment, which drive galaxy formation and evolution. It is thus possible to trace the evolution of the gaseous, stellar, and dark matter components, whose results in the literature have been shown to be in good agreement with observations (Nelson et al. 2018; Springel et al. 2018; Xu et al. 2019).

The model assumes a  $\Lambda$ CDM cosmology with  $\Omega_{\Lambda,0} = 0.6911$ ,  $\Omega_{\text{m},0} = 0.3089$ ,  $\Omega_{\text{b},0} = 0.0486$ ,  $\sigma_8 = 0.8159$ ,  $n_s = 0.9667$  and  $h = 0.6774$  (Planck Collaboration et al. 2016), that follows the evolution of the particles from  $z = 127$  to  $z = 0$ . For identifying structures and substructures, the friends-of-friends (FoF) group finder and the SUBFIND algorithm (Springel et al. 2001; Dolag et al. 2009) were used in all the snapshots, considering a linking length  $b = 0.2$  to identify bound particles. Subhalos with non-zero stellar components are labeled as galaxies. According to our selection criteria for the progenitors, we consider subhalos with stellar masses greater than 50 initial gas cells. In the case of dark matter (DM) particles, 50 particles were used as a threshold. The merger trees were constructed by SubLink (Rodríguez-Gomez et al. 2015) and LHalotree (Springel et al. 2005) and provided information about the assembly history of galaxies. Both SubLink and LHalotree identify all descendant connections that belong to the same FoF group. This leads to numerous branches within the galaxy history since each subhalo/galaxy can be linked to one or more progenitors. We have followed galaxies using the main progenitor branch, corresponding to the most massive progenitor identified at each timestep. Access to the data is public and available at [www.tng-project.org/](http://www.tng-project.org/).

For the purpose of this work, we use TNG300, corresponding to  $205 h^{-1} \text{ Mpc}$  of box length. The advantage of using TNG300 is that it follows the evolution of  $2500^3$  DM particles and gas cells simultaneously in the simulation. This number provides good statistics regarding massive structures.

### 2.2. MDPL2-SAG

The MDPL2-SAG galaxy catalog was constructed by combining the semi-analytic model of galaxy formation SAG (Cora et al. 2018) with the cosmological DM MULTIDARK PLANCK 2 simu-

lation, MDPL2 (Klypin et al. 2016; Knebe et al. 2018). The code includes the contribution of several physical processes, such as radiative gas cooling, quiescent star formation, starbursts triggered by mergers and disc instabilities, AGN and SNe (Type Ia and II) feedback, and chemical enrichment. Additionally, the code includes environmental effects like RPS *on satellites*, and gradual starvation. The model distinguishes two types of satellites. The first one corresponds to satellite galaxies that maintain their dark matter halos, whose dynamics allow for tracking galaxy orbits; and the second ones are ‘orphan galaxies’, differentiated from the former because their dark matter halos could not be identified by the halo finder, due to resolution effects. We have checked the contribution of these orphans to our sample, but most of the low-mass central galaxies selected in this study were not orphans in the past. The model assumes a  $\Lambda$ CDM cosmology with  $\Omega_m = 0.307$ ,  $\Omega_\Lambda = 0.693$ ,  $\Omega_B = 0.048$ ,  $n_s = 0.96$  and  $H_0 = 100 h^{-1} \text{km s}^{-1} \text{Mpc}^{-1}$ , where  $h = 0.678$  (Planck Collaboration et al. 2014), tracing the evolution of  $3840^3$  particles from  $z = 120$  to  $z = 0$  in a box of side length  $1 h^{-1} \text{Gpc}$ .

The ROCKSTAR halo finder (Behroozi et al. 2013b) was used to identify the DM halos and their substructures. This algorithm works with a phase-space based on the standard deviations of the particle distribution in position and velocity space, with a linking length of  $b = 0.28$ , guaranteeing that virial spherical overdensities can be determined for even the most ellipsoidal halos. In this context, any overdensities should comprise at least 20 DM particles. According to the selection criteria, central galaxies are identified as galaxies residing in the center of the potential well of massive host halos. These main structures can host multiple substructures called subhalos, where satellite galaxies reside. For merger trees, CONSISTENTTREES (Behroozi et al. 2013a) algorithm was used to build up the catalogs. The MDPL2 datasets can be found in the COSMOSIM database<sup>1</sup>.

For both catalogs, we focus on studying how the different properties of these galaxies change over time. We analyze various parameters such as the halo mass,  $M_{200}$ , which represents the mass within a radius  $R_{200}$  where the halo density is 200 times the critical density of the Universe. We also consider the maximum circular velocity ( $v_{\text{max}}$ ) representing the highest value of the spherically-averaged rotation curve, note the definition of this parameter changes according to the simulation (see Table 2); the stellar mass ( $M_\star$ ) of the subhalo/galaxy, the total gas mass ( $M_{\text{gas}}$ ) including both cold and hot components, and the specific star formation rate (sSFR) defined as the ratio of the star formation rate (SFR) to the stellar mass ( $M_\star$ ). Each parameter description can be found in Table 2.

### 3. Methodology

In this section, we describe and define the galaxy selection criteria and the samples used in this study.

#### 3.1. Target and Control samples

We selected all the low-mass central galaxies in the outskirts of massive systems ( $M_{200} \geq 10^{13} h^{-1} M_\odot$ ) up to  $5 h^{-1} \text{Mpc}$  of their centers at  $z = 0$ . The range in stellar mass is  $M_\star = [10^{9.5}, 10^{10}] h^{-1} M_\odot$  and it was chosen based on the results obtained in Lacerna et al. (2022), where they found a strong conformity signal from these central galaxies at  $z = 0$ . We call these galaxies the *target sample*. For TNG300 (MDPL2-SAG), 13,274 (2,495,308) central galaxies at  $z = 0$  were identified in the target sample.

Additionally, we chose a *control sample* with the same stellar mass range as the target sample, except that it was made of central galaxies located farther than  $5 h^{-1} \text{Mpc}$  from the centers of galaxy groups and clusters. This selection allowed us to assess whether the proximity to massive systems influences the behavior of low-mass central galaxies. The selection gave us 26,605 (3,814,590) central galaxies in the control sample of TNG300 (MDPL2-SAG). The target and control samples represent the entire sample of central galaxies in that stellar mass range within the catalogs at  $z = 0$ . For both samples, we follow their evolution until  $z = 2$ . To identify the TNG300 galaxies in the past, we followed the main progenitor branch for each treeID, which corresponds to the index of the FoF host/parent of each galaxy<sup>2</sup>. In other words, we traced their evolution using the SubhaloGrNr parameter. So, if  $t_{99}$  corresponds to the snapshot at  $z = 0$  (snapshot 99 in TNG300), we trace the galaxies backward in time using the previous time steps (e.g.,  $t_{91}$  for  $z = 0.1$ ); this enables us to follow the history of the previous subhalo (i.e. galaxy at snapshot  $t_{n-1}$ ) which shares the same descendant, corresponding to the most massive one derived from LHaloTree and so on. In the case of MDPL2-SAG, we follow the galaxies in the past using the GalaxyStaticID parameter which corresponds to the ID of each galaxy inside the simulation, which will be unique, independent of the simulation snapshot.

#### 3.2. Separating Q and SF galaxies

We separated the samples into quenched (Q) and star-forming (SF) galaxies at  $z = 0$  to follow their evolution separately. To do this, we consider the same sSFR cut used in Lacerna et al. (2022) to split the samples. In this way, a galaxy will be considered quenched if  $\text{sSFR} \leq 10^{-10.5} h \text{yr}^{-1}$ . From the target sample in TNG300, we find 2,142 ( $\sim 16\%$ ) quenched galaxies and 11,132 ( $\sim 84\%$ ) SF galaxies at  $z = 0$ , while for the control sample, we find 2,012 ( $\sim 8\%$ ) quenched and 24,593 ( $\sim 92\%$ ) SF galaxies. Table 3 gives all the information about both samples in IllustrisTNG300. For the target sample, we find a fraction significantly greater of quenched galaxies than in the control sample. For SF galaxies, in both cases, the percentages are greater than 80%, even for the target sample, suggesting that most of these galaxies are still forming new stars in environments close to massive systems.

For MDPL2-SAG, the Q and SF galaxies for both target and control samples were separated using the same sSFR cut at  $z = 0$ , as was established in TNG300. This value is also based on the results of Cora et al. (2018), where it was found to reproduce well the bimodality of galaxies within the simulation. From the target sample, we find 69,718 ( $\sim 3\%$ ) quenched galaxies and 2,425,590 ( $\sim 97\%$ ) SF galaxies, while for the control sample, we find 11,989 ( $\ll 1\%$ ) quenched and 3,802,601 ( $> 99\%$ ) SF galaxies. The differences in number are mostly given by the box size of the semi-analytic model which is significantly greater than TNG300 and therefore gives us better statistics in the mass range of this study. It is important to note that for the semi-analytic model, the percentages for Q galaxies are considerably lower compared to the fractions found in IllustrisTNG. Nonetheless, we find for the semi-analytic model a behavior similar to that in TNG300, where the number of SF low-mass central galaxies is greater than the number of quenched galaxies, which in the case of MDPL2-SAG increases to 97% for the target sample. Table 4 summarizes the properties of the target and control samples for MDPL2-SAG.

<sup>1</sup> <https://www.cosmosim.org/>

<sup>2</sup> Note that the IDs will not be identical in each snapshot.

Catalog	Parameter	Description	Column name*
IllustrisTNG300	$M_{200}$	Total mass of this group enclosed in a sphere whose mean density is 200 times the critical density of the Universe, at the time the halo is considered.	Group_M_Crit200
	$M_{\star}, M_{\text{gas}}$	Total mass of all member particle/cells which are bound to this Subhalo, separated by type. Particle/cells bound to subhaloes of this Subhalo are NOT accounted for.	SubhaloMassType
	SFR	Sum of the individual star formation rates of all gas cells in this subhalo.	SubhaloSFR
	$v_{\text{max}}$	Maximum value of the spherically-averaged rotation curve. All available particle types (e.g. gas, stars, DM, and supermassive black holes) are included in this calculation.	SubhaloVmax
MDPL2-SAG	$M_{200}$	Mass of the corresponding dark matter halo ( $M_{200}$ ) in Rockstar.	halomass
	$M_{\star}$	Mass of stars in the spheroid/bulge and the disk.	mstarspheroid + mstardisk
	$M_{\text{coldgas}}$	Mass of gas in the spheroid/bulge and the disk.	mcoldspheroid + mcolddisk
	$M_{\text{hotgas}}$	Hot gas mass.	mhot
	SFR	Star formation rate.	sfr
	$v_{\text{max}}$	Halo circular velocity in physical coordinates, frozen in orphan galaxies.	vmax

**Table 2.** Parameters taken from the public catalogs from IllustrisTNG and MDPL2 webpages.

\*Based on the column name given in each catalog.

TNG300	Target sample	Control sample
$\log_{10} M_{\star} [h^{-1} M_{\odot}]$	[9.5, 10]	[9.5, 10]
$N_{\text{gals}}$	13,274	26,605
$N_{\text{gals}} \text{ Q (at } z = 0)$	2,142 (16.1%)	2,012 (7.6%)
$N_{\text{gals}} \text{ SF (at } z = 0)$	11,132 (83.9%)	24,593 (92.4%)

**Table 3.** Properties of the target and control samples for IllustrisTNG300.

MDPL2-SAG	Target sample	Control sample
$\log_{10} M_{\star} [h^{-1} M_{\odot}]$	[9.5, 10]	[9.5, 10]
$N_{\text{gals}}$	2,495,308	3,814,590
$N_{\text{gals}} \text{ Q (at } z = 0)$	69,718 (2.8%)	11,989 (0.3%)
$N_{\text{gals}} \text{ SF (at } z = 0)$	2,425,590 (97.2%)	3,802,601 (99.7%)

**Table 4.** Properties of the target and control samples for MDPL2-SAG.

The above results support the theory that there are more star-forming galaxies in the low mass regime than quenched galaxies. The quenched fraction of galaxies increases when low-mass central galaxies are close to galaxy groups and clusters, but the fraction of SF galaxies still dominates.

### 3.3. Primary and secondary samples

Because we are also interested in studying the conformity signal, we have defined two other samples: *primary* and *secondary* samples. The idea is to analyze the correlation in the sSFR of low-mass central galaxies (primary galaxies) with their neighbors (secondary galaxies). The primary sample at  $z = 0$  corresponds to both target and control galaxies and the secondary sample is all the neighboring galaxies (either central or satellite) that inhabit within a radius of  $10 h^{-1}$  Mpc from the primary galaxies. Some authors argue that the inclusion of satellites in the secondary sample for the measurement of conformity can produce some contamination in the results, mainly because some surveys cannot distinguish properly between a central or satellite (Kauffmann et al. 2013, Sin et al. 2017, Tinker et al. 2017). However, satellite neighbors also play an important role in the signal measured. Because we are using simulated data, in this study we consider both central and satellite as secondary galaxies, which have stellar masses greater than  $10^9 h^{-1} M_{\odot}$ . This lower limit in the stellar mass has been used to avoid resolution effects in previous works (e.g., IllustrisTNG300: Pillepich et al. 2017, Montero-Dorta et al. 2020, Lacerna et al. 2022; MDPL2-SAG: Haggard et al. 2020, Hough et al. 2023). We applied this criterion in both simulations when measuring the two-halo conformity (Sec. 5).

We measured the mean quenched fraction ( $f_Q$ ) of all neighbor galaxies as a function of the distance from the primary samples (Q and SF primaries) until  $10 h^{-1}$  Mpc. The quenched fraction of neighbor galaxies is measured at different redshifts. We perform the analysis up to  $z = 1$  because of the low number of quenched, central galaxies in the stellar mass range of  $10^{9.5}$  to

Catalog	$z = 0$	$z = 0.3$	$z = 1$
IllustrisTNG300	39,879 (Q: 10.4%; SF: 89.6%)	41,036 (Q: 2.5%; SF: 97.5%)	37,680 (Q: < 0.1%; SF: > 99.9%)
<i>after removing fs</i>	37,535 (Q: 8.3%; SF: 91.7%)	39,603 (Q: 1.7%; SF: 98.3%)	37,372 (Q: << 0.1%; SF: > 99.9%)
MDPL2-SAG	6,309,898 (Q: 1.3%; SF: 98.7%)	5,309,100 (Q: <1%; SF: >99%)	3,753,659 (Q: <1%; SF: >99%)
<i>after removing fs</i>	6,243,666 (Q: 1.1%; SF: 98.9%)		

**Table 5.** Number of primary galaxies with  $M_*$  between  $10^{9.5}$  and  $10^{10} h^{-1} M_\odot$  at different redshifts for measuring the two-halo conformity. Each panel corresponds to IllustrisTNG300 and MDPL2-SAG galaxy catalogs, *before* and *after* removing former satellites (fs). Percentages of primary galaxies in the Q and SF samples are indicated in brackets.

$10^{10} h^{-1} M_\odot$  at higher redshifts. Table 5 summarizes properties of all the primary samples at three different redshifts ( $z = 0, 0.3,$  and  $1$ ) for both IllustrisTNG300 and MDPL2-SAG galaxy catalogs.

### 3.4. Former satellites

In addition, we have identified *former satellites* (fs) in each catalog. Given that TNG300 and MDPL2-SAG are different built galaxy catalogs, we have applied different criteria to select the former satellites. These definitions were applied to enhance the comprehension of the role of these galaxies in the signal of the two-halo conformity, mostly because previous work showed controversial results (see the Introduction). Furthermore, the criteria used were useful to avoid spurious former satellite classification given by the subhalo finder. For TNG300, we consider the information provided by the subhalo finder and add a distance criterion. We selected all the satellite candidates identified in one or more past snapshots and measured the distance between the satellite galaxy and their respective central galaxy at that time. If the distance satisfies  $d \leq 2R_{200}$ , the galaxy is considered a satellite in that snapshot, otherwise, it is considered central. For SAG, we also considered the information provided by the subhalo finder, and we paid attention to the existence of one more member in the respective (Rockstar) halo in that snapshot. We realized that there are cases where a central galaxy at present is flagged as a satellite in some snapshot(s) in the past by the halo finder, but there were no other galaxies in the same host halo (in that snapshot). Therefore, if the galaxy is a satellite according to the subhalo finder but it is the only one in the host halo, then the galaxy is still considered central by us. Otherwise, if there are other galaxies (either central, satellites, or orphans) in the same halo, the galaxy will be classified as a former satellite. For the two-halo conformity at higher- $z$  (Sec. 5.2), we have applied the same criteria (per model) to select former satellites, that is, selecting candidates that satisfy all the conditions mentioned above for the progenitors of primary galaxies at  $z = 0.3$  and  $z = 1$ .

## 4. The evolution of low-mass central galaxies

Our interest lies in studying the large-scale environmental effects on low-mass central galaxies located in the outskirts of groups and clusters. These effects may lead to their cessation of SF activity. Additionally, we aim to explore their potential contribution to the conformity signal at large scales. To achieve this, we present the evolutionary histories of these galaxies from the TNG300 and MDPL2-SAG datasets. Fig. 1 shows the evolution of the median trends of the host halo mass,  $M_{200}(z)$ , the stellar mass,  $M_*(z)$ , the total gas content,  $M_{\text{gas}}(z)$ , the specific star for-

mation rate,  $s\text{SFR}(z)$ , and the maximum circular velocity,  $v_{\text{max}}(z)$  from *left to right* for TNG300 (upper panel) and MDPL2-SAG (lower panel) catalogs. Each panel shows the evolution of Q (red) and SF (blue) target galaxies. The shaded contours correspond to the 16th and 84th percentiles for each sample. In addition, Figs. 2 and 3 show the same as in Fig. 1 but separating the Q (upper) and SF (lower) galaxies to compare the histories with the control sample which is shown in gray. In the following section, we will describe the analysis performed for each parameter of interest.

### 4.1. Analysis of physical parameters

#### 4.1.1. Host halo mass growth

One of our hypotheses regarding the star formation quenching of these low-mass central galaxies near massive halos involves the influence on their growth. To verify the existence of this effect, we examine the growth of the host halo mass of target and control galaxies. The left panel of Fig. 1 shows the evolution of the median  $M_{200}(z)$  for Q (red line) and SF (blue line) target galaxies. In addition, we have added the  $v_{\text{max}}$  parameter (halo circular velocity, *right* panel) as a dynamical mass proxy. For TNG300, SF galaxies were hosted by less massive halos than Q galaxies, at least down to  $z \sim 0.3$ , where the lines converge mostly to the same median values. At this redshift, there is a considerable fraction of Q galaxies that inhabited more massive halos (see the shaded region), with masses above  $10^{13} h^{-1} M_\odot$  (its 84th percentile is about  $10^{14} h^{-1} M_\odot$ ). This trend was not observed for SF galaxies. At lower redshifts, there is a steep drop in halo growth for the Q galaxies, reaching a median value of  $\log_{10}(M_{200}/h^{-1} M_\odot) = 11.394$  at  $z = 0$ . We see in Fig. 2 that the host halo mass growth for the control sample is quite different than the Q targets at lower redshifts, reaching a higher median value of  $\log_{10}(M_{200}/h^{-1} M_\odot) = 11.524$  at  $z = 0$ . The growth of the halo mass in SF galaxies evolves monotonically in both target and control samples, and resembles the trend observed in Q control galaxies. The median value for SF galaxies in the target sample reaches  $\log_{10}(M_{200}/h^{-1} M_\odot) = 11.549$  at  $z = 0$ , being slightly lower than SF control galaxies, which reach a median value of  $\log_{10}(M_{200}/h^{-1} M_\odot) = 11.582$ .

On the other side, for MDPL2-SAG we find that SF galaxies evolve inhabiting less massive halos than their Q counterpart, at least until  $z \sim 0.3$  (same behavior found in TNG300). At lower redshifts, the median trend for Q target galaxies drops dramatically, increasing the differences between the host halos from Q and SF target galaxies at  $z = 0$ , with median values of  $\log_{10}(M_{200}/h^{-1} M_\odot) = 10.997$  and  $11.468$ , respectively. Figure 3 shows that the rapid drop in the host halo mass occurs only for target galaxies, i.e. those ones inhabiting the outskirts of galaxy groups and clusters. For control galaxies in MDPL2-SAG, the

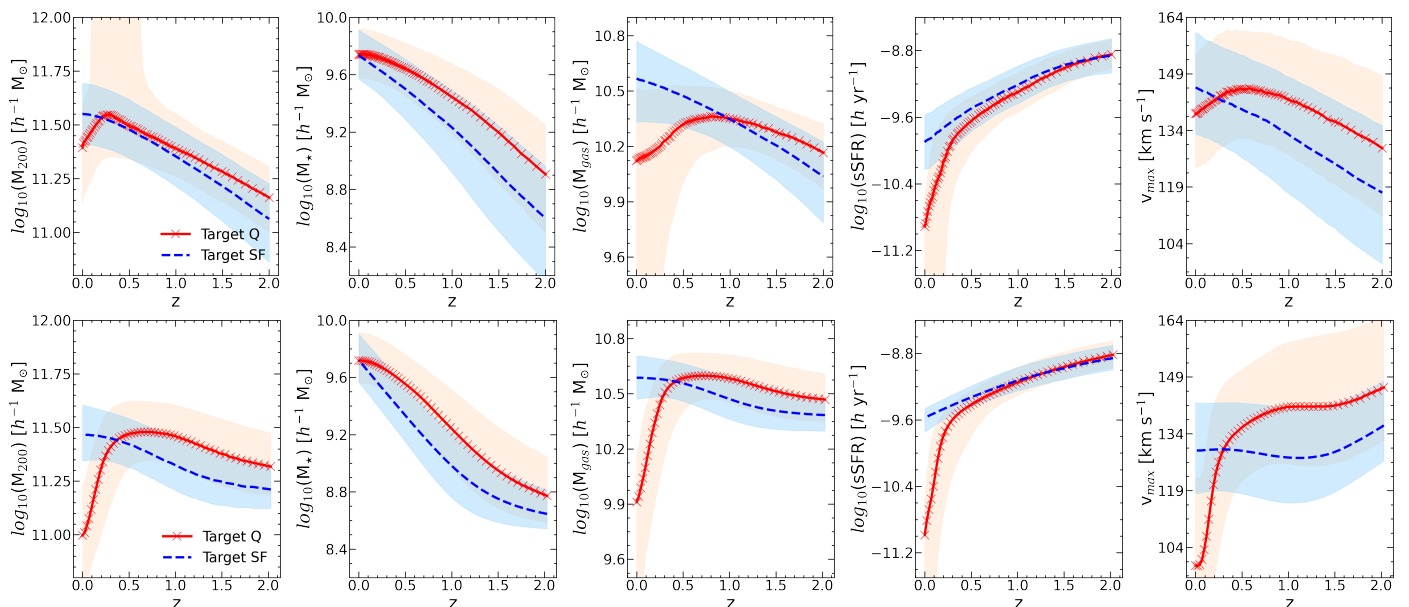


**Fig. 1.** Median trends of the target sample from TNG300 (top) and MDPL2-SAG (bottom). From left to right:  $M_{200}(z)$ ,  $M_*(z)$ ,  $M_{\text{gas}}(z)$ ,  $\text{sSFR}(z)$  and  $v_{\text{max}}(z)$ . The red and blue lines represent the Q and SF samples, respectively. The shaded regions indicate the 16th–84th percentile ranges.

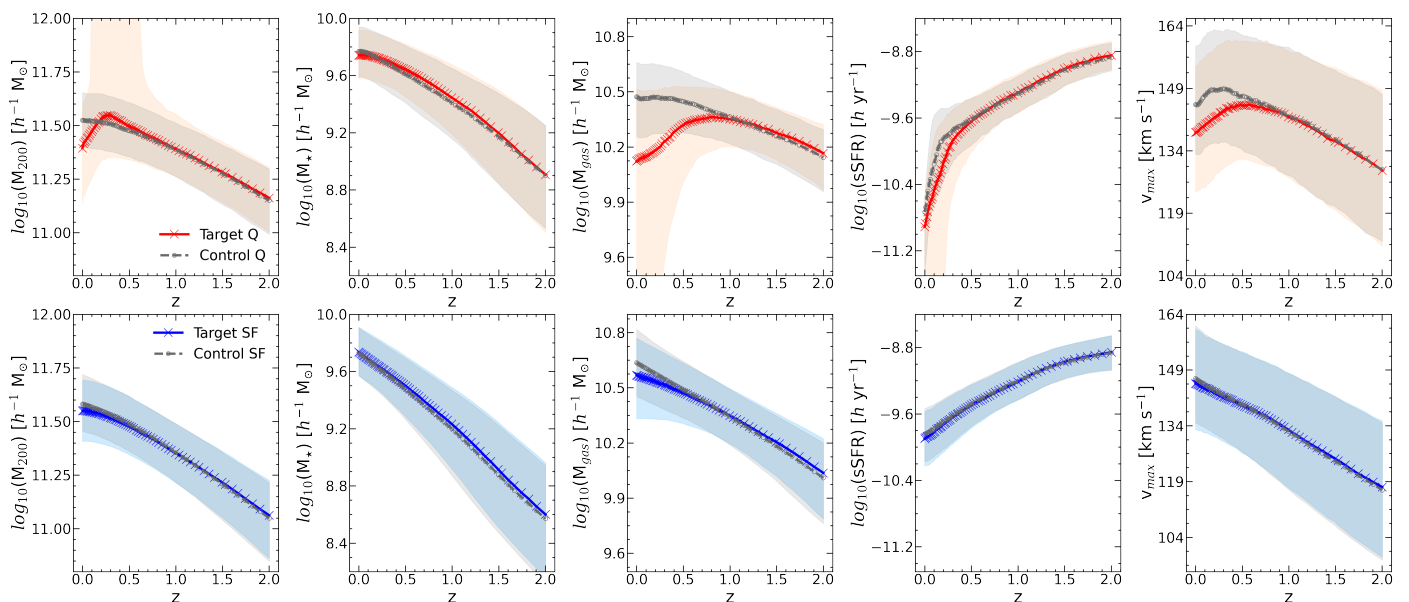


**Fig. 2.** Same parameters as Fig. 1. The upper panels show the median trends for Q galaxies (target sample in red, control sample in gray) and the lower panels show the SF galaxies for the target (blue) and control (gray) samples in TNG300.

median trend is qualitatively similar to those found for control galaxies in TNG300. For Q control galaxies, the median value at  $z = 0$  is  $\log_{10}(M_{200}/h^{-1} M_{\odot}) = 11.574$ . In the case of SF galaxies, small differences are found at  $z > 0.5$ , where target galaxies are hosted in slightly more massive DM halos than SF control objects. And when reaching  $z = 0$  the trend is reversed, with a median value of  $\log_{10}(M_{200}/h^{-1} M_{\odot}) = 11.498$  for control galaxies.

An interesting difference found between both models is that for the MDPL2-SAG, we have not found target galaxies that would have been hosted by massive halos with masses  $M_{200} \geq 10^{13} h^{-1} M_{\odot}$  in the past.

In the case of  $v_{\text{max}}$ , quenched target galaxies in TNG300 show a peak around  $z \sim 0.5$  followed by a drop (similar as found

for  $M_{200}$ ). This behavior does not occur for MDPL2-SAG, instead  $v_{\text{max}}$  slightly decreases until  $z \sim 0.5$ , followed by a steep drop in their median values. Both models in turn show control quenched galaxies with larger  $v_{\text{max}}$  values than Q targets at present (see upper-right panels in Figs. 2 and 3). In the case of SF target galaxies, each model shows evolutionary histories comparable to their control samples, showing no major differences concerning the location of these galaxies with respect to groups or clusters. However, we find different evolutions for this parameter if we compare the models. It monotonically increases for SF galaxies in TNG300, while for MDPL2-SAG,  $v_{\text{max}}$  decreases and then shows a flatter behavior at  $z < 1$ .

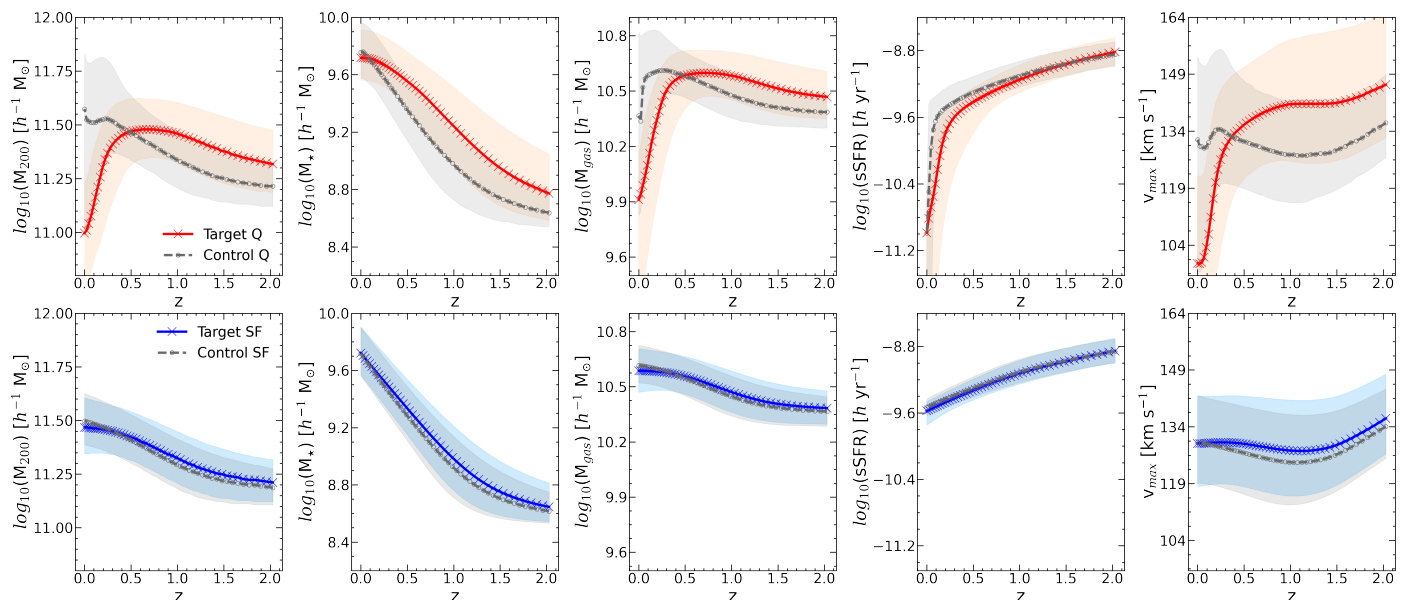


**Fig. 3.** Same parameters as Fig. 1. The upper panels show the median trends for Q galaxies (target sample in red, control sample in gray), and the lower panels show the SF galaxies for the target (blue) and control (gray) samples in MDPL2-SAG.

#### 4.1.2. Evolution of the gas and stellar mass content

The second and third panels of Fig. 1 show the evolution of the stellar mass and total gas content, respectively.

For stellar masses, the median trends in TNG300 and MDPL2-SAG are quite similar. Q galaxies exhibit a higher stellar mass over the whole  $z$  range than SF galaxies. If we compare the median trends with the control samples (see Figs. 2 and 3), indeed, the evolutionary paths are almost indistinguishable for TNG300. The median values at  $z = 0$  reach  $\log_{10}(M_{\star}/h^{-1} M_{\odot}) = 9.740$  and  $9.734$  for Q and SF target galaxies, and  $\log_{10}(M_{\star}/h^{-1} M_{\odot}) = 9.769$  and  $9.730$  for Q and SF control galaxies, respectively. In the case of MDPL2-SAG, some distinction can be seen during the stellar mass evolution, being Q target galaxies slightly richer in stellar mass than Q control galaxies (see upper panel of Fig. 3). The median trends for SF target and control (see lower panel of Fig. 3) remain quite similar as in TNG300. The values at  $z = 0$  reach  $\log_{10}(M_{\star}/h^{-1} M_{\odot}) = 9.717$  and  $9.720$  for Q and SF target galaxies, and  $\log_{10}(M_{\star}/h^{-1} M_{\odot}) = 9.756$  and  $9.718$  for Q and SF control galaxies.

For the evolution of the gas content, the Q galaxies in TNG300 reach a maximum around  $z \sim 1$  and then decrease their amount until  $z = 0$ . The 16th percentile and median comparison with the control sample (Fig. 2) shows that the gas content loss becomes more important for those galaxies in the outskirts of massive groups and clusters, increasing this gap at  $z = 0$ . The median values for the target galaxies are  $\log_{10}(M_{\text{gas}}/h^{-1} M_{\odot}) = 10.122$  and  $10.568$  for Q and SF galaxies. In the case of control galaxies, the median values reach  $\log_{10}(M_{\text{gas}}/h^{-1} M_{\odot}) = 10.473$  and  $10.636$  for Q and SF galaxies, respectively.

The scenario in MDPL2-SAG, on the other hand, shows that Q target galaxies experienced more gas loss than their SF counterpart, which drives the quenching of these galaxies at  $z = 0$ . The drop in gas mass is even more dramatic compared to TNG300, a similar behavior as found for the host halo mass in Q galaxies. This behaves similarly to the findings by Salerno et al. (2022), where galaxies in infall and filamentary regions exhibit a drop in the mass of hot gas from  $z \sim 0.5$  to the present.

The median values in the gas mass at  $z = 0$  for the target galaxies are  $\log_{10}(M_{\text{gas}}/h^{-1} M_{\odot}) = 9.911$  and  $10.587$  for Q and SF galaxies. If we compare the median trends with the control sample, no major differences are found for SF galaxies. Instead, Q control galaxies exhibit a slight drop in the last snapshots, which was not observed in TNG300. The median values for control galaxies reach  $\log_{10}(M_{\text{gas}}/h^{-1} M_{\odot}) = 10.367$  and  $10.616$  for Q and SF galaxies.

As a summary of the gas mass, both TNG300 and MDPL2-SAG galaxy catalogs qualitatively follow the same trend in the evolution of galaxies inhabiting near massive groups and clusters. For the control galaxies, small differences arise mainly in the gas mass for the quenched galaxies.

#### 4.1.3. sSFR history

Since low-mass central galaxies in the vicinity of massive systems appear to be more quenched than those galaxies inhabiting regions farther than  $5 h^{-1}$  Mpc at  $z = 0$ , we follow their sSFR history to estimate if these differences were milder in the past. The fourth panel (from left to right) of Fig. 1 shows the median sSFR history of both Q and SF galaxies. Both synthetic catalogs show a decreasing evolutionary trend until  $z = 0$ . At higher  $z$ , Q and SF samples have very similar median values of sSFR, but after  $z \sim 1.5$  in TNG300 (upper panel) and  $z \sim 1$  in SAG (lower panel), the evolutionary paths start to diverge, where the Q galaxies exhibit a steeper drop compared to the SF counterpart. We can notice from both models that this drop in sSFR of Q galaxies is independent of the distance of these galaxies to a group or cluster, which can be seen clearly in Figs. 2 and 3 where Q target galaxies are compared with Q control galaxies.

Interestingly, at  $z \sim 0.3$  the slope of Q galaxies in both simulations becomes steeper dropping to  $\text{sSFR} \sim 10^{-11} h \text{ yr}^{-1}$  at  $z = 0$ . This behavior might be connected to the drop in the host halo mass growth.

Given that the target and control samples have stellar masses between  $\log_{10}(M_{\star}/h^{-1} M_{\odot}) = [9.5, 10]$  at  $z = 0$ , we are aware that there might be resolution problems at higher redshifts. How-

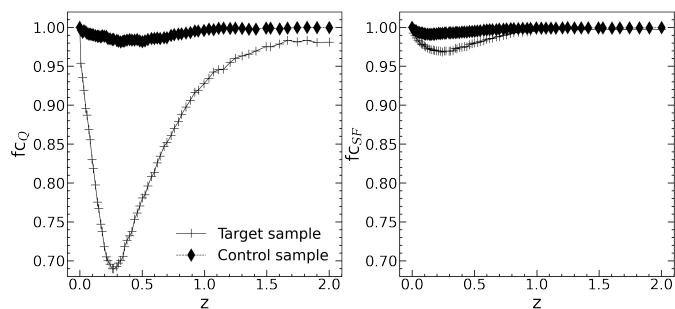


**Fig. 4.** Evolution in the fraction of central galaxies for Q (left) and SF (right) galaxies of the target and control samples in TNG300 (crosses and diamonds, respectively). The fraction is equal to unity at  $z = 0$  by definition.

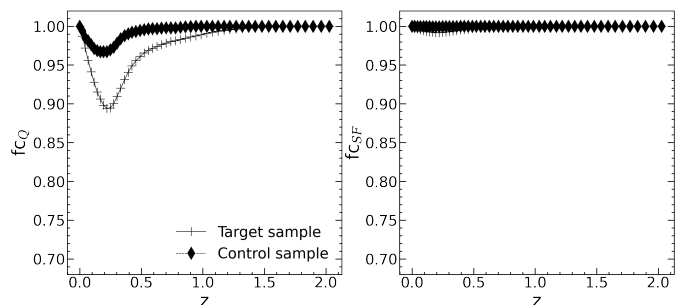


**Fig. 5.** Same as Fig. 4, but for the target and control samples in MDPL2-SAG.

ever, we have shown that our important results occur at  $z < 1$  where typically the progenitor stellar masses are  $> 10^9 h^{-1} M_{\odot}$ , so that resolution effects should not affect the analysis of the evolution of these galaxies.

#### 4.2. Removing former satellites

As previous studies have shown (e.g., Ayromlou et al. 2023 and Wang et al. 2023), it has been demonstrated that former satellites contribute to the two-halo conformity signal, but with controversial results about their impact. This highlights the importance of suitable sampling of former satellites (we detail the definitions used in this study in §3.4). The results in the previous section on the halo mass growth showed that a significant fraction of Q target galaxies were hosted by massive DM halos at  $z \sim 0.3$  in TNG300. This phenomenon could suggest that a fraction of low-mass central galaxies may have previously been satellites of more massive systems, which influenced their properties during that time. In order to assess this effect, we first analyzed how the fraction of low-mass central galaxies ( $f_c$ ) changed in the past for both TNG300 and MDPL2-SAG catalogs. By definition,  $f_c = 1$  at  $z = 0$ ; if their progenitors were always central galaxies, then  $f_c = 1$  at all redshifts. Figures 4 and 5 show how the fraction of central galaxies for the target (crosses) and control (diamonds) samples varied at different epochs during their evolution in each catalog. As we can see in the figures, a significant fraction of Q galaxies (left panels) were satellites at some time in the past, reaching a maximum at  $z \sim 0.3$  in both models, with about 30% of the targets for the hydrodynamical model and 11% for the semi-analytic model at that time. The identification of former satellites is done in halos of any mass, but these results elucidate the observed trend in TNG300 in which a significant fraction of Q target galaxies were hosted by more massive DM halos. In the case of Q control galaxies, the percentages reach around 4% at

TNG300	SAG			
	$N_{fs}$	%	$N_{fs}$	%
Target Q	967	45.1%	11,899	17.1%
Target SF	766	6.9%	46,663	1.9%
Control Q	72	3.6%	678	5.7%
Control SF	539	2.2%	6,997	0.2%

**Table 6.** Number of former satellites,  $N_{fs}$ , and the corresponding percentages for target and control samples separated into star-forming (SF) and quenched (Q) galaxies.

that epoch for TNG300, indicating it is more likely that galaxies have been part of other hosts in the past if they are inhabiting regions close to massive groups or clusters. For SF galaxies, the percentages of central galaxies that were satellites in the past are quite low compared to the quenched sample, which decreases even more if the galaxy belongs to the control sample.

The cumulative percentages of former satellites at  $z = 0$  found for TNG300 are 45% (Q) and 7% (SF) for target galaxies, and 4% (Q) and 2% (SF) for the control sample. Instead, for MDPL2-SAG, 17% (Q) and 2% (SF) were satellites for the target sample, and 6% (Q) and less than 1% (SF) for the control galaxies. All this information is summarized in Table 6.

It is important to notice that for Q target galaxies of each model, a significant percentage was satellite in the past, which might be associated with the distance of these galaxies to other massive structures. However, SF target galaxies do not show significant percentages of former satellites even when these galaxies are located near massive halos as well. Probably, most of the former satellites became quenched systems by environmental processes when they belonged to another halo. For all galaxies in the control samples, the maximum percentage of former satellites reaches 6% for control Q sample in the semi-analytic model, decreasing the percentage for the other sub-samples. Given that around half of the Q low-mass central galaxies in TNG300 were satellites in the past, we traced the evolution of low-mass central galaxies by removing these former satellites. With this, we aim to understand the role of these objects in the results of the previous section. The results are as follows.

For TNG300, we find that the main differences between the target sample before and after removing former satellites come from the host halo mass growth;  $v_{max}$ , being consistent with the observed behavior in  $M_{200}$ ; and the gas content for Q galaxies at  $z \lesssim 1$ . We show these parameters in Fig. 6. Their median trends (red lines) show a more flattened evolution, compared to the previous trends found in Fig. 1, in which we had a drop during the last stages of their evolution. Therefore, the drop in halo and gas mass was produced by former satellites. If we compare how the trends look with respect to the control galaxies (gray lines), we can still find slight differences at lower redshift, where target galaxies show lower median values than control ones, showing this flattened behavior on the host halo mass and gas mass in the quenched target galaxies. The stellar mass and sSFR parameters do not change whether the galaxy belongs to the target or the control sample, once the former satellites are excluded. For SF galaxies, on the other hand, the median trends appear to not change significantly after removing these galaxies. Moreover, given the small number of former satellites found in this sample, this seems not to influence the SF activity, because they

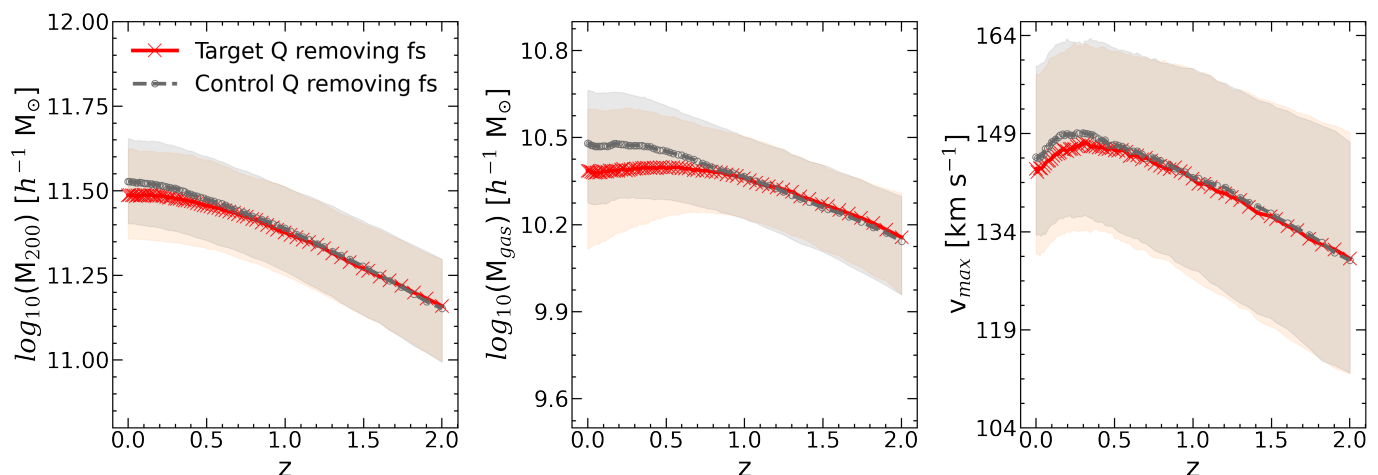


**Fig. 6.** Evolution of the host halo mass (*left*), gas mass (*middle*), and  $v_{\max}$  (*right*) for the target and control Q galaxies, after removing former satellites in TNG300.

are still forming stars at present. In fact, the median trends for target and control SF galaxies are quite similar to those in Fig. 2, for this reason, we have decided not to include these figures. This means that before or after removing former satellites, at least for SF galaxies, the median trends for galaxies in regions near massive systems will have evolutionary histories similar to those of galaxies in regions farther from massive groups or clusters. For MDPL2-SAG, the median trends for Q and SF galaxies, either from the target or the control sample, do not show differences when former satellites are removed from the analysis (see Appendix A). For SF galaxies, this behavior could be explained by the low number of former satellites (less than 2%) on those samples. However, for Q galaxies the percentages are greater, reaching 17% for Q target galaxies. We expected that by removing the former satellites in the target sample, the evolutionary trends of the gas and halo mass would be comparable to their control sample, as the results obtained from TNG300. However, the halo mass,  $v_{\max}$ , and gas mass still exhibit a drop at low redshift, leading to noticeable differences between the samples. One explanation could be related to the fact that all former satellites found in the semi-analytic model were inhabiting less massive halos, in comparison to those former satellites identified in TNG300. This behavior can be seen clearly in the lower-left panel of Fig. 1. Moreover, this behavior is quite similar to the results obtained for the SF galaxies of TNG300, in which we do not have a large fraction of galaxies that inhabited massive halos to alter the median trends on their evolution. Then, its trends remain the same, which is what we have seen for all the galaxies in MDPL2-SAG.

In summary, the former satellite galaxies only show an important contribution to the evolution of the halo mass and gas mass of the Q target galaxies in TNG300. The next section will present the analysis of their contribution to the signal of two-halo conformity. Based on the results of this section, we expect the Q target galaxies that were satellites in the past can explain a significant part of the conformity signal in TNG300, but the situation is less clear in the case of MDPL2-SAG.

## 5. Conformity signal

In the literature, only a few studies have been carried out to analyze the influence of former satellites on the two-halo conformity signal, from which inconclusive results have been obtained on this matter, as we have previously mentioned. In this section, we use the samples of primary and secondary galaxies defined

in Sec. 3.3 to measure the conformity, and analyze the contribution of former satellites to the signal in the local universe and at higher- $z$ .

### 5.1. Conformity signal in the local universe

Figure 7 shows the conformity signal at  $z = 0$  for TNG300. The upper panel shows the mean quenched fraction ( $f_Q$ ) of all neighbor galaxies of the Q and SF primary samples (red and blue solid lines, respectively) until separations of  $10 h^{-1}$  Mpc. The dashed lines correspond to the  $f_Q$  after removing former satellites from the primary sample. Since the primary galaxies are target plus control galaxies, we have removed all former satellites regardless of whether they are target or control galaxies. The lower panel shows the conformity signal, that is, the difference in the  $f_Q$  of all neighbor galaxies at a given distance from the Q and SF primary samples, before (black solid line) and after (gray dashed line) removing former satellites from the primary sample. We estimated the uncertainties in the mean  $f_Q$  using the Jackknife method by dividing the simulation in 8 subboxes. For this, we calculated the standard deviation per unit bin distance by removing a single subbox at a time. Therefore, the errors in the mean quenched fraction correspond to the standard deviation from the 8-subboxes. Given the large number of secondary galaxies, the error bars are small enough to be imperceptible in some of these figures.

By construction, the solid lines in Fig. 7 correspond to the trends found in Lacerna et al. (2022) for the same stellar mass range of primaries using TNG300, while the dashed lines correspond to the new results in this study. In the lower panel, it can be seen that the signal is low at distances larger than  $4 h^{-1}$  Mpc after removing former satellites from the primary sample. However, between 1 and  $4 h^{-1}$  Mpc, there are signs of conformity, i.e., the Q fraction of neighboring galaxies still depends on the sSFR of the primary galaxy. Thus, we could say that the signal at  $z = 0$  is strongly influenced by former satellites in the past. However, it cannot be fully explained by these galaxies.

This result is qualitatively consistent with the results obtained in Ayromlou et al. (2023, see their Fig. 8), for which the conformity signal is lower when former satellites are removed from the analysis using the LGal-A21 semi-analytic model.

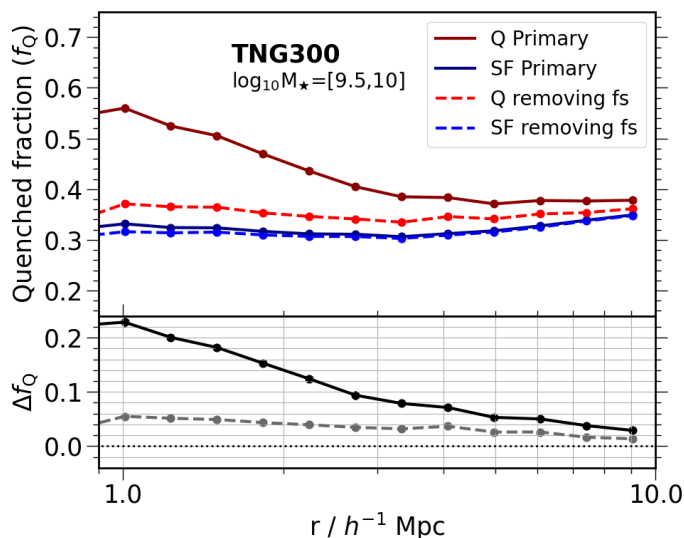


**Fig. 7.** Conformity signal in TNG300 at  $z = 0$ . The upper panel shows the mean quenched fraction of secondary galaxies for both quenched (red) and star-forming (blue) primary galaxies *before* (solid lines) and *after* (dashed lines) removing former satellites. The bottom panel shows how the conformity signal varies *before* (black solid line) and *after* (gray dashed line) removing former satellites, until  $10 h^{-1}$  Mpc distances from primary galaxies.

However, they estimate that the contribution of former satellites to the signal goes up to 20%, and decreases at larger scales. In our study, the former satellites in TNG300 contribute 75% (1 - the ratio between gray and black lines in the lower panel of Fig. 7) of the signal at  $1 h^{-1}$  Mpc and decrease from 70% to 50% between 2 and  $4 h^{-1}$  Mpc. Our results are more similar to those obtained with TNG300 by Wang et al. (2023, see their Fig. 6), in which the authors attributed all the two-halo conformity signal to former satellite galaxies. It is important to note that their study only considered central galaxies as neighbors, so the role of neighboring satellites was not included in the measured signal, which might explain the differences of 25–50% in the contribution of former satellites compared with those authors. We have performed the test considering only central galaxies for the secondary sample at  $z = 0$ , and the results (see Fig. B.1) showed their overall contribution is about 67% of the conformity signal at scales between 1 and  $2 h^{-1}$  Mpc. In other words, the former satellite contribution appears to strongly depend on the methodology and model used (see Appendix B for further discussion when using only central galaxies as neighbors).

Figure 8 shows the mean quenched fractions of secondary galaxies around primary galaxies using the MDPL2-SAG model at  $z = 0$ . The errors in  $f_Q$  are estimated using the diagonal of the covariance matrix after splitting every sample into 120 subsamples. Again, the error bars are very small given the large number of secondary galaxies. Although  $f_Q$  values for the fiducial cases (red and blue solid lines) are different from those in TNG300, they are qualitatively similar. Moreover, the conformity signal (black solid line in the lower panel) is quantitatively similar between both simulations, something already pointed out in Lacerna et al. (2022), but in this case, using exactly the same stellar mass range for the primaries. The conformity signal does not change after removing former satellite galaxies in the semi-analytic model (grey dashed line), though. This result is consistent with the unchanged evolution of the physical properties of low-mass central galaxies in MDPL2-SAG after removing the

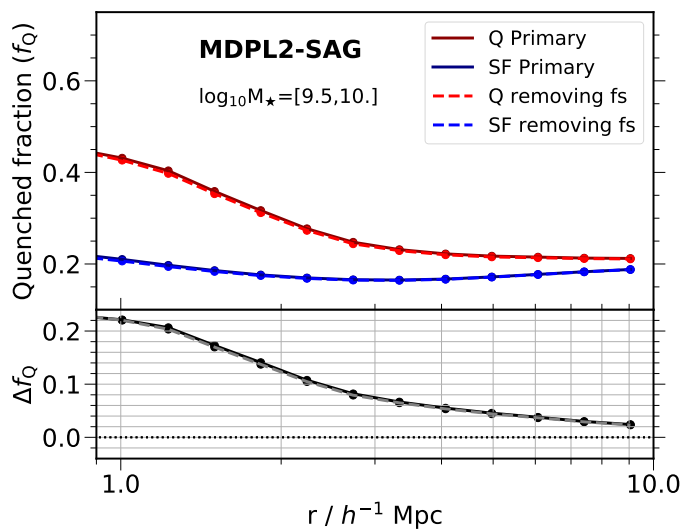


**Fig. 8.** Conformity signal in MDPL2-SAG at  $z = 0$ . The lines are the same as those described in Fig 7.

former satellites. Again, the contribution of the former satellites to the conformity signal strongly depends on factors such as methodology and technical properties of the simulations, which explain the differences found between the results from Ayromlou et al. (2023) and Wang et al. (2023).

## 5.2. Conformity signal at higher redshifts

We have seen that the two-halo conformity signal at  $z = 0$  is partly driven by former satellite galaxies in TNG300. These results evidence the importance of these galaxies in the measured signal. Although former satellites mostly explain the conformity signal, there is still some signal between  $1 - 4 h^{-1}$  Mpc that remains. Here, we analyze how the signal behaves at higher redshift, to visualize their impact along the evolution. We have selected two snapshots in our study,  $z \sim 0.3$  and  $z \sim 1$ . This selection was made based on our previous results, in which we found interesting trends at  $z \sim 0.3$  (halo mass) and  $z \sim 1$  (gas mass), showing significant changes in the evolution of quenched, low-mass central galaxies in the outskirts of massive systems, whose behavior is associated to former satellites. At  $z \sim 1$ , in addition, the results can be directly compared with those from Ayromlou et al. (2023).

Figures 9 and 10 are similar to Fig. 7 but show the conformity signal at  $z \sim 0.3$  and  $z \sim 1$ , respectively, for TNG300. From both figures, we can see that the signal (black solid line) increases significantly compared with that at  $z = 0$ , which suggests that the growth of the conformity signal is a function of redshift, being in good agreement with Ayromlou et al. (2023) for this simulation. At  $z \sim 0.3$ , the signal significantly decreases after removing former satellites. The gray dashed line shows some signal between 1 and  $4 h^{-1}$  Mpc, the same distance bin with a residual signal found at  $z = 0$ . We measure that, at  $z \sim 0.3$ , former satellites contribute to the conformity signal up to 85%. This could tell us that some other environmental process could be acting on the conformity signal at these scales but with lower importance, at least in TNG300. On the other side, if we analyze the signal at  $z \sim 1$ , and then remove the former satellites, the signal disappears, because all quenched, low-mass central galaxies were identified as satellites at least once in the past ( $z > 1$ ). This sce-

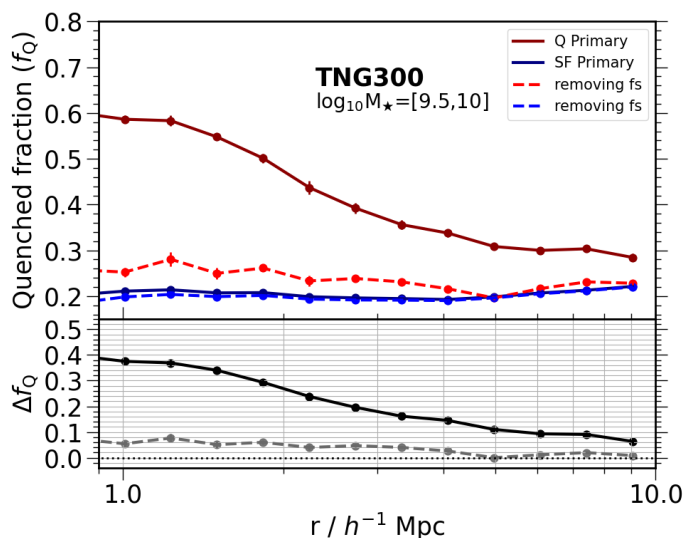


Fig. 9. Same as Fig. 7, but at  $z \sim 0.3$ .

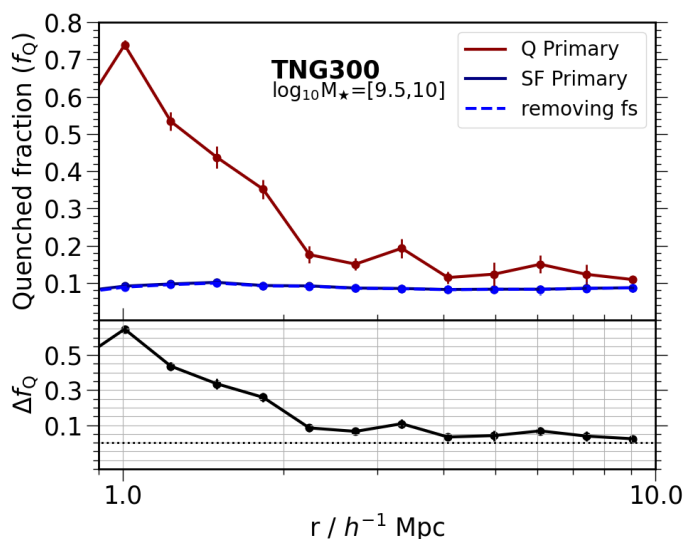


Fig. 10. Same as Fig. 7, but at  $z \sim 1$ .

nario was proposed by Wang et al. (2023) where they find that all the conformity signal at  $z = 0$  comes from these former satellite galaxies. However, as we have seen, the signal disappears completely at  $z = 1$  but it does not disappear completely at lower redshift.

Figure 11 summarizes the fiducial cases for the conformity signal at three different redshifts in the semi-analytic model. We have decided to compare in a single figure the fiducial conformity signals in MDPL2-SAG since former satellites in this model do not contribute to the signal. At  $z = 0.3$  (dashed line), there is a slight enhancement of the signal at scales smaller than  $2 h^{-1}$  Mpc with respect to the case at  $z = 0$  (solid line). However, at distances larger than  $2 h^{-1}$  Mpc from primary galaxies, both lines are inverted, showing more correlation at present. If we analyze the signal at  $z = 1$  (dotted dashed line), we can see the signal decreases over the whole range of distances. This result contradicts the findings in TNG300 for the fiducial case, in which we found the signal grows as a function of redshift, but there is a better agreement when the former satellites are removed in

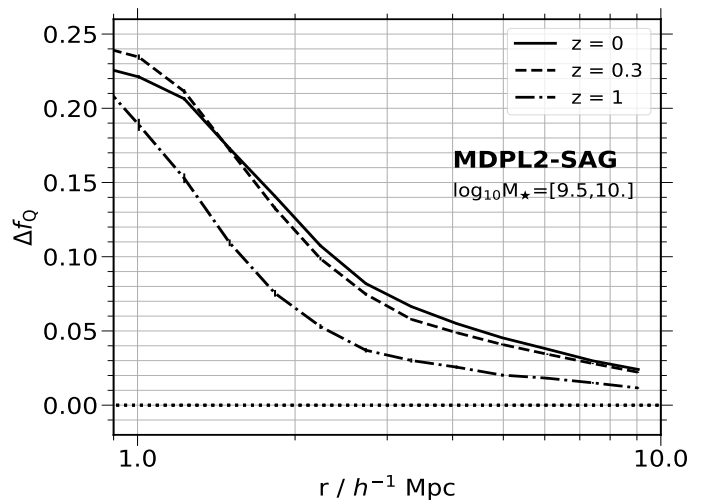


Fig. 11. Same as the lower panel of Fig. 8. Conformity signal in MDPL2-SAG at three different epochs:  $z = 0$  (solid line), 0.3 (dashed line) and 1 (dotted dashed line).

the hydrodynamic simulation. From the literature, we can compare our results with Ayromlou et al. (2023). Using an updated version of the L-Galaxies semi-analytic model, they found the signal decreases from  $z = 0$  to  $z = 2$ , showing an enhancement at  $z = 1$  compared with  $z = 0$ . In our case, the smaller amplitude of the conformity signal in the MDPL2-SAG model at  $z = 1$  than that in the present is comparable with their findings using the EAGLE simulation. As discussed by those authors, the time evolution of the signal is complex, and the different results might come from the impact of the physical properties involved in each model. We also point out the contribution of former satellites, given by the construction and characteristics of each simulation, in their respective evolution of the conformity signal.

## 6. Discussion and conclusions

We have seen from previous studies (e.g., Lacerna et al. 2022, Ayromlou et al. 2023) that low-mass central galaxies ( $M_* = [10^{9.5}, 10^{10}] h^{-1} M_\odot$ ) in the vicinity of galaxy groups and clusters can produce a strong two-halo conformity signal, that is, the correlation in sSFR between the central galaxy and their neighboring galaxies (either central or satellite galaxies). We have analyzed how the physical properties of these low-mass central galaxies (‘target’ galaxies) evolve from  $z = 2$  to the present using the hydrodynamical simulation IllustrisTNG300 and the semi-analytic galaxy catalog MDPL2-SAG to find hints about the origin of this signal. For that, we have separated into quenched (Q) and star-forming (SF) galaxies at  $z = 0$ . We have also considered central galaxies of the same stellar mass located farther from the center of massive systems (‘control’ galaxies). In addition, we have analyzed how former satellites, i.e., central galaxies at present but that were satellites in the past, can influence the median trends in the overall evolution of low-mass central galaxies, as well as assess their contribution to the conformity signal. Our main results are:

- The evolution of halo mass and gas mass parameters for low-mass quenched central galaxies in the vicinity of massive groups and clusters reveals a significant drop in their median values at  $z \lesssim 1$ , attributed to the presence of former satellites in TNG300. We also find a decline in halo and gas mass (and

$v_{\max}$ ) in quenched target galaxies of MDPL2-SAG; however, this drop is not associated with former satellites. The drop in halo mass for Q target galaxies is not observed in the control sample of quenched galaxies in both simulations. For SF galaxies instead, no major differences are found between target and control galaxies during their evolution.

- After removing former satellites on TNG300, the median trends of halo mass, gas mass, and  $v_{\max}$  for Q target galaxies exhibit similar trends compared to Q control galaxies (Fig. 6). However, small differences arise at lower redshifts, showing slightly lower median values in these parameters for target galaxies, with a flatter behavior from  $z < 0.5$  for halo mass and gas mass. In contrast, galaxies from MDPL2-SAG show no evident variations in their evolutionary histories once the former satellite galaxies were removed. Therefore, the differences found between Q target and Q control galaxies remain for this catalog.
- The percentages of former satellites for both TNG300 and MDPL2-SAG are higher for Q galaxies, reaching respectively 45% and 17% for Q target galaxies and less than 7% for SF target galaxies.
- Most of the former satellites in Q target galaxies appear to be hosted by massive dark matter halos ( $M_{200} \geq 10^{13} h^{-1} M_{\odot}$ ) in TNG300. However, the scenario in MDPL2-SAG is quite different, showing all former satellites to be hosted by less massive halos, with mean halo masses around  $10^{11} h^{-1} M_{\odot}$ .
- Former satellites play an important role in the two-halo conformity signal in TNG300. At higher redshift ( $z \sim 1$ ), these galaxies can explain the whole signal, while at lower redshifts ( $z \lesssim 0.3$ ), they contribute up to 75 – 85% to the signal. Therefore, around 15 – 25% of the conformity signal comes from other processes at  $z \lesssim 0.3$  in this simulation. The contribution of former satellites in the two-halo conformity is negligible in MDPL2-SAG.
- The time evolution of the conformity signal at Mpc scales is apparently contradictory in both simulations. The signal decreases from  $z = 0$  to  $z = 1$  in MDPL2-SAG, while it increases in TNG300. However, after removing former satellites in the latter, the signal practically does not change at  $z \leq 0.3$ , and it disappears at  $z = 1$ .

The TNG300 and MDPL2-SAG synthetic galaxy catalogs are very different because the physical processes involved may act in different ways on the galaxies or the efficiency of these processes is not the same. Thus, it is expected to find quantitative differences in the evolution of low-mass galaxy properties such as stellar mass, gas mass, and sSFR. Nonetheless, the results presented in this study show that these properties are qualitatively similar in both simulations (see Figs. 1–3). The inherent differences between TNG300 and MDPL2-SAG are manifested in the different mean quenched fractions of neighbor galaxies around the low-mass central objects at  $z = 0$ . However, the two-halo conformity signal, i.e., the difference in the quenched fraction of neighbor galaxies at a given distance from the Q and SF low-mass centrals, is very similar in both simulations (black solid lines in Figs. 7 and 8). Therefore, the conformity signal is mostly independent of the differences in the physical processes between both galaxy catalogs. As shown by Lacerna et al. (2022) and Ayromlou et al. (2023), most of this signal comes from central galaxies near massive galaxy groups and clusters, i.e., the target galaxies. The quenched target galaxies produce an excess of correlation between them and quenched neighboring galaxies. Why are those low-mass target galaxies quenched? After checking the evolution histories of their physical properties, including

those related to their host DM halo, and comparing them with the low-mass central galaxies of control, we can conclude that there is no single explanation for the quenching of target galaxies in both simulations.

We have found that in the case of TNG300, 75–85% of the two-halo conformity signal comes from target galaxies that were hosted by massive dark matter halos in the past. According to Ayromlou et al. (2023), former satellite galaxies can lose gas and dark matter due to stripping inside and in the outskirts of their former host halos. We add that this is more likely to occur for low-mass central galaxies that were satellites in massive halos (see also Wetzel et al. 2014), which naturally explains the quenching in their star formation activity. Our results about the two-halo conformity in TNG300 are qualitatively consistent with the results found in Ayromlou et al. (2023) using the L-Galaxies semi-analytic model because, in both studies, former satellites at  $z = 0$  can explain part of the signal but not all. In the case of the study performed by Wang et al. (2023), although they found that the signal could be explained by central galaxies that were satellites in the past in the TNG300 simulation, they used only central galaxies as secondary galaxies. If we contrast our results with their study (Appendix B), we can infer that part of the conformity signal comes from the secondary sample of satellite-type galaxies (and not only from central neighbors) around Q primary galaxies. In addition, we have tested the importance of the former satellite definition, which should be considered carefully, in the sense that it can lead to different results, due to cases of misclassification of former satellite galaxies by the halo finder.

In contrast, we did not find low-mass central galaxies accreted by massive halos in the past in MDPL2-SAG. The former satellites do not contribute to the two-halo conformity measured in this catalog. Therefore, the most likely explanation for the excess of correlation in sSFR between quenched target galaxies and their quenched neighbor galaxies in TNG300 is not applied to the targets in MDPL2-SAG. The remarkable drop in  $M_{200}$  since  $z \sim 0.46$  for Q targets, followed by the drops in  $M_{\text{gas}}$  and sSFR since  $z \sim 0.43$  and 0.28, respectively (Fig. 3), suggest that the tidal stripping of halo mass by massive neighbor halos (Hahn et al. 2009) can be responsible for the quenching of the target galaxies in MDPL2-SAG, which in turn may explain the two-halo conformity in this catalog.

Since the host halos of central target galaxies have not been part of a larger system before, the severe mass stripping could also be due to tidal forces in the ‘cosmic web’ (Borzyszkowski et al. 2017; Montero-Dorta & Rodriguez 2024). For example, tidal forces in galaxy clusters have been found to be quite efficient at disrupting smaller systems, such as groups, by removing their satellites (e.g., Choque-Challapa et al. 2019, Hagggar et al. 2023), so we might expect something similar to happen in dense, large-scale structures such as thick filaments. An in-depth study about the role of filaments in the mass stripping of low-mass halos in the vicinity of groups and clusters will be addressed elsewhere.

*Acknowledgements.* We would like to thank Nelson Padilla, Tomás Hough, Vladimir Avila-Reese, Sergio Contreras, and Yetli Rosas-Guevara for useful comments and discussions. We also thank Yamila Yaryura and Cristian Vega for their support to organize and provide the MDPL2-SAG data used in this work. MCA acknowledges support from ANID BASAL project FB210003. SAC acknowledges funding from *Consejo Nacional de Investigaciones Científicas y Tecnológicas* (CONICET, PIP-2876), and *Universidad Nacional de La Plata* (G11-183), Argentina. FR thanks the support by *Agencia Nacional de Promoción Científica y Tecnológica*, the *Consejo Nacional de Investigaciones Científicas y Técnicas* (CONICET, Argentina) and the *Secretaría de Ciencia y Tecnología de la Universidad Nacional de Córdoba* (SeCyT -UNC, Argentina). FR would like to

acknowledge support from the ICTP through the Junior Associates Programme 2023-2028. DP acknowledges financial support from ANID through FONDECYT Postdoctorado Project 3230379. DP, gratefully acknowledges support by the ANID BASAL project FB210003. NCC acknowledges a support grant from the Joint Committee ESO-Government of Chile (ORP 028/2020).

## References

- Abadi, M. G., Moore, B., & Bower, R. G. 1999, *MNRAS*, 308, 947
- Abazajian, K. N., Adelman-McCarthy, J. K., Agüeros, M. A., et al. 2009, *ApJS*, 182, 543
- Aragon-Salamanca, A., Ellis, R. S., Couch, W. J., & Carter, D. 1993, *MNRAS*, 262, 764
- Ayromlou, M., Kauffmann, G., Anand, A., & White, S. 2023, *MNRAS*, 519, 1913
- AYROMLOU, M., KAUFFMANN, G., YATES, R. M., NELSON, D., & WHITE, S. D. M. 2021, *MNRAS*, 505, 492
- BAHÉ, Y. M., MCCARTHY, I. G., BALOGH, M. L., & FONT, A. S. 2013, *MNRAS*, 430, 3017
- BALOGH, M. L., NAVARRO, J. F., & MORRIS, S. L. 2000, *ApJ*, 540, 113
- BEHROOZI, P. S., WECHSLER, R. H., & WU, H.-Y. 2013a, *ApJ*, 762, 109
- BEHROOZI, P. S., WECHSLER, R. H., WU, H.-Y., ET AL. 2013b, *ApJ*, 763, 18
- BLANTON, M. R., SCHLEGEL, D. J., STRAUSS, M. A., ET AL. 2005, *AJ*, 129, 2562
- BORZYSZKOWSKI, M., PORCIANI, C., ROMANO-DÍAZ, E., & GARALDI, E. 2017, *MNRAS*, 469, 594
- CHOQUE-CHALLAPA, N., SMITH, R., CANDLISH, G., PELETIER, R., & SHIN, J. 2019, *MNRAS*, 490, 3654
- CORA, S. A., VEGA-MARTÍNEZ, C. A., HOUGH, T., ET AL. 2018, *MNRAS*, 479, 2
- DOLAG, K., BORGANI, S., MURANTE, G., & SPRINGEL, V. 2009, *MNRAS*, 399, 497
- FORMAN, W. & JONES, C. 1982, *ARA&A*, 20, 547
- FUJITA, Y. 2004, *PASJ*, 56, 29
- GIOVANELLI, R. & HAYNES, M. P. 1985, *ApJ*, 292, 404
- GUNN, J. E. & GOTT, J. RICHARD, I. 1972, *ApJ*, 176, 1
- HAGGAR, R., GRAY, M. E., PEARCE, F. R., ET AL. 2020, *MONTHLY NOTICES OF THE ROYAL ASTRONOMICAL SOCIETY*, 492, 6074–6085
- HAGGAR, R., KUCHNER, U., GRAY, M. E., ET AL. 2023, *MNRAS*, 518, 1316
- HAHN, O., PORCIANI, C., DEKEL, A., & CAROLLO, C. M. 2009, *MNRAS*, 398, 1742
- HAINES, C. P., PEREIRA, M. J., SMITH, G. P., ET AL. 2015, *ApJ*, 806, 101
- HOUGH, T., CORA, S. A., HAGGAR, R., ET AL. 2023, *MNRAS*, 518, 2398
- KAUFFMANN, G., LI, C., ZHANG, W., & WEINMANN, S. 2013, *MNRAS*, 430, 1447
- KLYPIN, A., YEPES, G., GÖTTLÖBER, S., PRADA, F., & HESS, S. 2016, *MNRAS*, 457, 4340
- KNEBE, A., STOPPACHER, D., PRADA, F., ET AL. 2018, *MNRAS*, 474, 5206
- LACERNA, I., RODRIGUEZ, F., MONTERO-DORTA, A. D., ET AL. 2022, *MNRAS*, 513, 2271
- LARSON, R. B., TINSLEY, B. M., & CALDWELL, C. N. 1980, *ApJ*, 237, 692
- LOPES, P. A. A., RIBEIRO, A. L. B., & BRAMBILA, D. 2024, *MNRAS*, 527, L19
- MAN, A. & BELLI, S. 2018, *NATURE ASTRONOMY*, 2, 695
- MARINACCI, F., VOGELSBERGER, M., PAKMOR, R., ET AL. 2018, *MNRAS*, 480, 5113
- MCCARTHY, I. G., FRENK, C. S., FONT, A. S., ET AL. 2008, *MNRAS*, 383, 593
- MONTERO-DORTA, A. D., ARTALE, M. C., ABRAMO, L. R., ET AL. 2020, *MONTHLY NOTICES OF THE ROYAL ASTRONOMICAL SOCIETY*, 496, 1182
- MONTERO-DORTA, A. D. & RODRIGUEZ, F. 2024, *MNRAS*, 531, 290
- MOORE, B., GOVERNATO, F., QUINN, T., STADEL, J., & LAKE, G. 1998, *ApJ*, 499, L5
- MOORE, B., KATZ, N., LAKE, G., DRESSLER, A., & OEMLER, A. 1996, *NATURE*, 379, 613
- MOORE, B., LAKE, G., QUINN, T., & STADEL, J. 1999, *MNRAS*, 304, 465
- NAIMAN, J. P., PILLEPICH, A., SPRINGEL, V., ET AL. 2018, *MNRAS*, 477, 1206
- NELSON, D., PILLEPICH, A., SPRINGEL, V., ET AL. 2018, *MNRAS*, 475, 624
- NELSON, D., SPRINGEL, V., PILLEPICH, A., ET AL. 2019, *COMPUTATIONAL ASTROPHYSICS AND COSMOLOGY*, 6, 2
- NEWBERG, H. J., YANNY, B., ROCKOSI, C., ET AL. 2002, *ApJ*, 569, 245
- PALLERO, D., GÓMEZ, F. A., PADILLA, N. D., ET AL. 2019, *MNRAS*, 488, 847
- PENG, Y., MAIOLINO, R., & COCHRANE, R. 2015, *NATURE*, 521, 192
- PILLEPICH, A., NELSON, D., HERNQUIST, L., ET AL. 2017, *MONTHLY NOTICES OF THE ROYAL ASTRONOMICAL SOCIETY*, 475, 648
- PILLEPICH, A., SPRINGEL, V., NELSON, D., ET AL. 2018, *MNRAS*, 473, 4077
- PIRAINO-CERDA, F., JAFFÉ, Y. L., LOURENÇO, A. C., ET AL. 2024, *MNRAS*, 528, 919
- PLANCK COLLABORATION, ADE, P. A. R., AGHANIM, N., ET AL. 2014, *A&A*, 571, A16
- PLANCK COLLABORATION, ADE, P. A. R., AGHANIM, N., ET AL. 2016, *A&A*, 594, A13
- POOLE, G. B., MUTCH, S. J., CROTON, D. J., & WYITHE, S. 2017, *MNRAS*, 472, 3659
- RODRIGUEZ-GOMEZ, V., GENEL, S., VOGELSBERGER, M., ET AL. 2015, *MNRAS*, 449, 49
- RUIZ, A. N., MARTÍNEZ, H. J., COENDA, V., ET AL. 2023, *MNRAS*, 525, 3048
- SALERNO, J. M., MURIEL, H., COENDA, V., ET AL. 2022, *MONTHLY NOTICES OF THE ROYAL ASTRONOMICAL SOCIETY*, 517, 4515
- SARRON, F., ADAMI, C., DURRET, F., & LAIGLE, C. 2019, *A&A*, 632, A49
- SIN, L., LILLY, S., & HENRIQUES, B. 2017, IN *GALAXY EVOLUTION ACROSS TIME*, 40
- SPRINGEL, V. 2010, *MNRAS*, 401, 791
- SPRINGEL, V., PAKMOR, R., PILLEPICH, A., ET AL. 2018, *MNRAS*, 475, 676
- SPRINGEL, V., WHITE, S. D. M., JENKINS, A., ET AL. 2005, *NATURE*, 435, 629
- SPRINGEL, V., WHITE, S. D. M., TORMEN, G., & KAUFFMANN, G. 2001, *MNRAS*, 328, 726
- TECCE, T. E., CORA, S. A., TISSERA, P. B., ABADI, M. G., & LAGOS, C. D. P. 2010, *MONTHLY NOTICES OF THE ROYAL ASTRONOMICAL SOCIETY*, 408, 2008
- TINKER, J. L., WETZEL, A. R., CONROY, C., & MAO, Y.-Y. 2017, *MNRAS*, 472, 2504
- VILLALOBOS, Á., DE LUCIA, G., & MURANTE, G. 2014, *MNRAS*, 444, 313
- WANG, H. Y., MO, H. J., & JING, Y. P. 2007, *MNRAS*, 375, 633
- WANG, K., PENG, Y., & CHENG, Y. 2023, *MNRAS*, 523, 1268
- WEINBERGER, R., SPRINGEL, V., HERNQUIST, L., ET AL. 2017, *MNRAS*, 465, 3291
- WETZEL, A. R., TINKER, J. L., & CONROY, C. 2012, *MNRAS*, 424, 232
- WETZEL, A. R., TINKER, J. L., CONROY, C., & VAN DEN BOSCH, F. C. 2013, *MNRAS*, 432, 336
- WETZEL, A. R., TINKER, J. L., CONROY, C., & VAN DEN BOSCH, F. C. 2014, *MNRAS*, 439, 2687
- XU, D., ZHU, L., GRAND, R., ET AL. 2019, *MNRAS*, 489, 842
- ZINGER, E., DEKEL, A., KRAVTSOV, A. V., & NAGAI, D. 2018, *MNRAS*, 475, 3654

## Appendix A: Evolution of central galaxies after removing former satellites in MDPL2-SAG

For completeness, Fig. A.1 shows the evolution in the properties of low-mass central galaxies in the MDPL2-SAG catalog after removing former satellites. The trends are quite similar to those shown in Fig. 3.

## Appendix B: Two-halo conformity considering only central galaxies as the secondary sample

As mentioned in the text, Wang et al. (2023) presented results where the former satellites can explain all the two-halo conformity signal in TNG300 at  $z \sim 0$ . A difference in that work compared to others is that they used only central galaxies in the sample of secondary galaxies. Fig. B.1 shows the results using that methodology, i.e., considering only central galaxies as the neighbor sample around primary galaxies. Compared to Fig. 7, the  $f_Q$  for the Q primaries in the fiducial case (red solid line) is lower, while  $f_Q$  for the SF primaries (blue solid line) is similar, which produces a lower two-halo conformity signal (black solid line). The  $f_Q$  values shown in solid lines in Fig. B.1 are consistent with those reported by Wang et al. (2023) in their Fig. 6 for the same stellar mass range. The conformity signal also decreases when the former satellites are not considered in the primary sample (grey dashed line), but it is not completely absent between 1 and  $2 h^{-1}$  Mpc in contrast to the results of those authors. We find that the former satellites contribute 67% of the two-halo conformity signal at these scales.

The difference in the contribution of former satellites to the conformity signal between this study and Wang et al. (2023) likely stems from the methodology to select them. In their case, the main progenitors of these central galaxies were once satellites of other halos and the satellite state lasts at least two successive snapshots. We checked there were cases in which a central galaxy at  $z = 0$  was clearly a satellite in the past just in a single snapshot, so we preferred to not use the condition of the satellite status in two successive snapshots. In our case, we considered a distance condition in which, at a given snapshot, a satellite candidate at  $d \leq 2 R_{200}$  from the host halo of the central galaxy is considered a former satellite, otherwise, it is considered central. The reason for this is that in TNG300 a galaxy can be associated with two different halos simultaneously in the same snapshot, either by late stages of a merger or ejected cores (see, e.g., Poole et al. 2017), with different distances from the host halos, one at the center and other at  $d > 0$ , and in both cases it can be flagged as central by the subhalo finder. Then, in the following snapshot(s), the galaxy can be flagged as satellite at  $d > 0$ . We noted that in a snapshot where the satellite candidate is at  $d > 2 R_{200}$ , and after checking its evolution in previous and following snapshots, it is likely an artifact of the subhalo finder to flag it as a satellite since they never crossed the virial radius of another halo. Therefore, in those cases, the galaxy is flagged as central by us. Wang et al. (2023), on the other hand, might have considered these galaxies as former satellites. Since these central galaxies are in the vicinity of massive structures, they might contribute significantly to the conformity signal as shown in Lacerna et al. (2022). This could explain why these authors concluded that the entire signal originates from ‘backsplash’ objects.

We consider our criteria for identifying former satellites to be reliable, and this is supported by checking that the evolution of target galaxies in TNG300 is more similar to that of control galaxies when the former satellites are removed (Sec. 4.2).

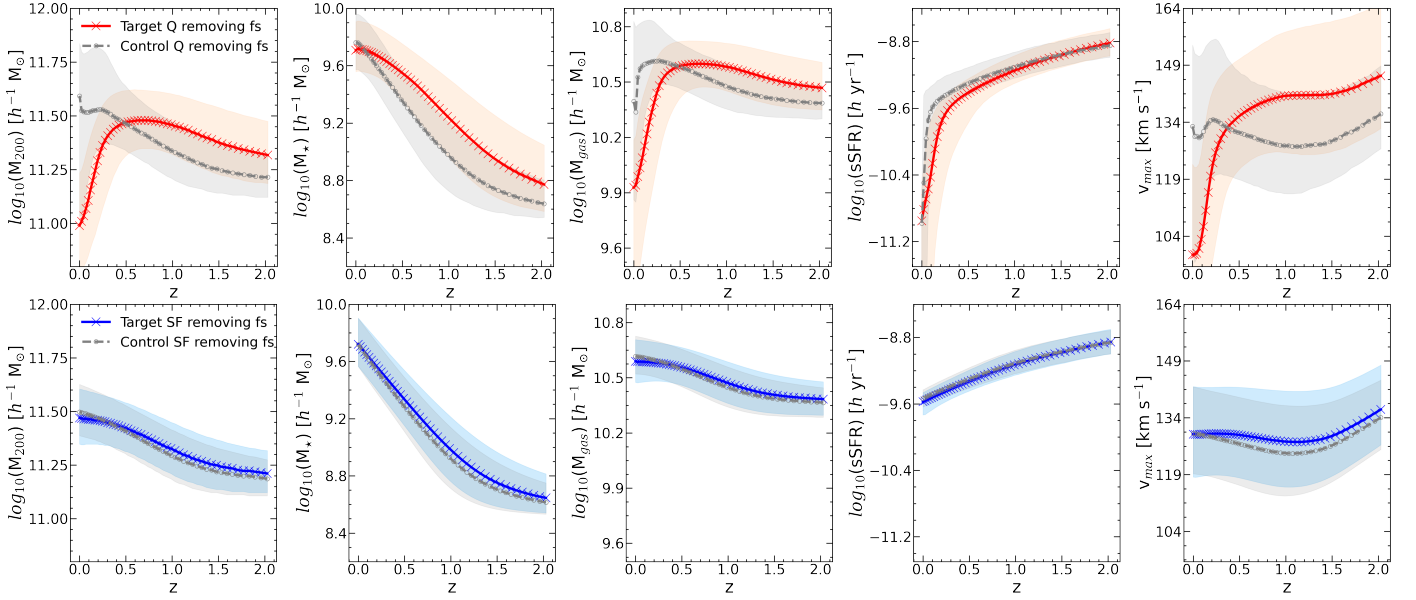


**Fig. A.1.** Same parameters as Fig. 3. The upper panels show the median trends for Q galaxies (target in red, control in gray), and the lower panels show the SF galaxies for the target (blue) and control (gray) samples in MDPL2-SAG, *after* removing former satellites.

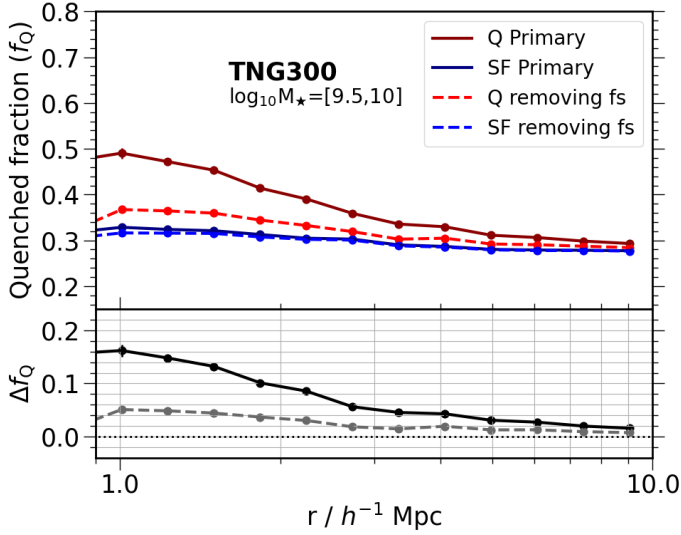


**Fig. B.1.** Same as Fig. 7, but considering *only centrals* as neighbor galaxies, similar as Wang et al. (2023).